The thermoelastic surface strip source for laser-generated ultrasound

A. Aharoni,[a] K. M. Jassby,[b] and M. Tur
Ultrasonics & NDT Laboratory, Faculty of Engineering, Tel Aviv University, Ramat Aviv, Tel Aviv 69978, Israel

(Received 25 March 1992; accepted for publication 18 August 1992)

The vertical ultrasonic surface displacement generated by a laser-induced, thermoelelastic, rectangular surface strip source is formulated. The main features of this source, ultrasonic rise times comparable to those of the generating light pulse derivatives, and a large amplitude, double-pulsed waveform, are advantageous for ultrasonic spectral- and time-domain measurements for nondestructive material evaluation. The analysis shows that, for laterally symmetric sources in the thermoelastic regime, only one tangential thermoelastic stress component contributes to the vertical displacement. Therefore, the strip source is equivalent to two, tangential line forces acting outward at the strip's front and back edges. The leading-edge rise time of the signal is virtually independent of the lateral extent of the source, which mostly affects the trailing portions of the ultrasonic pulses. Consequently, a particularly simple expression, which compares favorably with experimental results, is obtained for short strips (subtending small angles at the observation point). In conjunction with this formulation, the thermoelastic strip source is an important tool for quantitative, laser-based, ultrasonic nondestructive material evaluation.

PACS numbers: 43.35.Zc, 43.35.Ud

INTRODUCTION

The generation of acoustic waves by transient laser heating has seen increasing application in ultrasonic nondestructive testing.[1] This approach alleviates several drawbacks characteristic to the standard contact transducers. Wideband acoustic signal generation, nonobtrusive transduction of the ultrasound, improved scanning ability, and a potential for remote operation are the major advantages. Typically, Gaussian distributed point or line laser illumination patterns were used for this purpose.[1,2] The present authors have demonstrated faster rise times and larger amplitudes, with comparable laser pulses, by using a sharply defined rectangular illumination, or strip source.[3,4] This technique offers improved accuracy for time- and frequency-domain measurements, which are important for material evaluation. This paper analyzes the laser-based thermoelastic strip source, providing insight into its main characteristics. A theoretical model for the acoustic waveform generated by such a thermoelastic strip is formulated. This model serves as a reference for analyzing experimental data in laser-based material evaluation procedures.[4]

One of the first models for laser-generated ultrasound was derived by White.[5] His one-dimensional model considered the thermoelastic loading of metal surfaces for both isolated laser pulses and periodic pulse bursts. Later, distinction was drawn between the ablative regime, where material is blown-off the surface, and the thermoelastic regime, where only heating occurs without material phase changes.[6–9] Using numerical solutions for the free-surface Green's function, Scruby *et al.*[8] derived one of the first three-dimensional models for ultrasonic generation in solids.[8,9] Despite an idealized point source approximation to the experimental illumination spot, this model correctly predicts the salient features of experimental waveforms. It was established that an ablative source is equivalent to vertical momentum loading, whereas horizontal loading is expected in the thermoelastic regime.[10]

Analytic expressions for material displacements due to a thermoelastic *point* source were developed by Rose[11] for two observation points: along the vertical, epicentral axis, and on the surface. Several workers were then able to extend Rose's solution to finite line[12] and Gaussian sources[13,14] by convolving point-source-induced waveforms over the extended source dimensions. In a different approach, the acoustic waves generated by an extended axisymmetric (disk) source were calculated by direct solution of the relevant wave equations with the aid of integral transform techniques.[15] Much like the point source, extended sources have been shown to be equivalent to horizontal or vertical surface loading for the thermoelastic and ablative regimes, respectively. Other workers were able to obtain solutions for the two dimensional problem in a half-space for the thermoelastic regime,[16–18] as well as the ablative regime,[16,19] but these are not strictly valid for observation points on the free surface.

In the present work, the thermoelastic strip source geometry is analyzed. Rather than convolving available results for the thermoelastic point source, the analysis is performed from first principles, yielding a particularly simple expres-

[a] Present address: Department of Electrical Engineering, Stanford University, Stanford, CA 94305-4035.
[b] Present address: Inspection Research & Technologies, P. O. Box 39805, Tel Aviv 61397, Israel.

 0001-4966/92/123249-10$00.80

sion which circumvents the computational load associated with previous finite source models. The mathematical formulation for the surface displacement (Sec. I) takes the advantage of closed-form expressions for the free-surface displacement Green's functions for a transient point load. The extended surface thermoelastic strip source is replaced with its equivalent, two outward acting tangential line sources, to obtain an integral representation for the resulting surface displacements (Sec. I C). By approximating to a short strip source (subtending a small angle at the observation point), particularly simple expressions, are obtained (Sec. I D). Long strips are also considered (Sec. I E), showing that the lateral extent of the source has negligible effect on the leading portions of the ultrasonic waveform, but progressively changes the trailing signal as the source's length increases. The theoretical model is compared to experimental signals (Sec. II), and its significance is discussed in Sec. III.

I. THEORETICAL

Of the two major laser-based mechanisms for ultrasound generation:[8] the ablative, and the thermoelastic, only the latter is considered here. This mode dominates as long as the surface heating is insufficient to change the material phase (laser flux under some 10^7 W/cm^2 in metals[1]). The main macroscopic effect in the thermoelastic regime is a transient, localized surface heating, inducing local thermal stresses, which propagate in the form of ultrasonic waves, including several surface components. The thermoelastic mechanism is normally favored for nondestructive testing applications as it avoids ablative marring of the test surface. We consider here only the *vertical* surface displacement; other displacement components can be evaluated in a similar manner.

The thermoelastic surface strip source is analyzed using uncoupled thermoelastic theory. This simplification is justified[20] by the small mechanical coupling term in the heat conduction equation for metals (2.9% for aluminum and 1.4% for steel), and since the thermal and stress rates of change are comparable, as verified by a more refined analysis for practical situations.[21]

A. Integral representation for surface displacements

Consider a finite, transient thermal volume source, within an isotropic, homogeneous half-space occupying the $+z$ axis region (Fig. 1). The transient thermal load induces a transient mechanical load within the material which then propagates as an acoustic disturbance. Such an extended thermal source can be described with the aid of the thermal stress glut, $\Delta\tau_{ij}(\boldsymbol{\xi},t)$, which is the conceptual stress associated with the strain of the heated material volume [see Eq. (5)] were it removed from the constraining media,[22] and which is defined by

$$\Delta\tau_{ij}(\boldsymbol{\xi},t) \equiv C_{ijkl}\Delta e_{kl}(\boldsymbol{\xi},t) \,. \tag{1}$$

Here, $\Delta e_{kl}(\boldsymbol{\xi},t)$ denotes the stress-free thermal strain, C_{ijkl} is the elastic constant tensor and $\boldsymbol{\xi} = (\xi,\eta,\zeta)$ represents a Cartesian coordinate system at the source. As described by Bachus and Mulcahy,[22] the effective load of an extended source

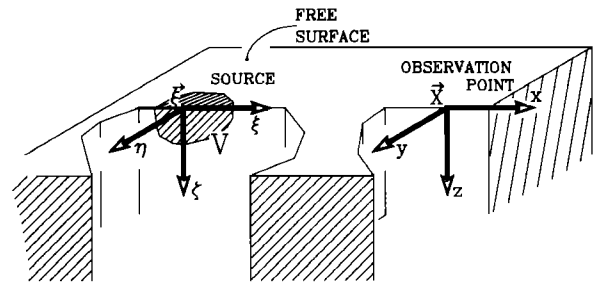

FIG. 1. Thermoelastic source geometry. The vertical surface displacement u_3 at $\mathbf{X}$ due to a volume thermal source at $\boldsymbol{\xi}$ is sought.

of volume V is equivalent to a combination of its body force modified by the derivative of the glut $-\Delta\tau_{ij,j}$ plus the surface traction acting on the source's envelope S, modified by the normal component of the stress glut $+\Delta\tau_{ij}\hat{n}_j$. Since no external tractions are present here and the true body forces are neglibible, the vertical surface displacement u_3 at a distant observation point $\mathbf{X} = (x,y,z)$ is given by

$$u_3(\mathbf{X},t) = -\int_V \Delta\tau_{ij,j}(\boldsymbol{\xi},t) * G^{\delta}_{3i}(\boldsymbol{\xi},t;\mathbf{X},0)\,dV + \int_S \Delta\tau_{ij}(\boldsymbol{\xi},t)\hat{n}_j * G^{\delta}_{3i}(\boldsymbol{\xi},t;\mathbf{X},0)\,dS \,, \tag{2}$$

where the effective volumetric load is weighted by the displacement Green's functions, $G^{\delta}_{3i}(\boldsymbol{\xi},t;\mathbf{X},0)$, representing the vertical displacement (in direction 3) at the observation point $\mathbf{X}$, due to a point force with delta function time excitation, acting at $\boldsymbol{\xi}$ in direction i. Summation over repeated indices is implied, the asterisk $(*)$ denotes convolution in time: $f*g = \int_0^t f(t')g(t-t')\,dt'$, and the comma in the subscript represents differentiation. Physical initial conditions are assumed, that is $(\partial/\partial t)G^{\delta}_{3i} = G^{\delta}_{3i} = 0$ for $t \leqslant 0$ in conjunction with the restriction, $\mathbf{X} \neq \boldsymbol{\xi}$.

Previous workers,[11,14] applied the divergence theorem, to replace the surface integral in Eq. (2) with an equivalent volume integral, such that[23]

$$u_3(\mathbf{X},t) = \int_V \Delta\tau_{ij}(\boldsymbol{\xi},t) * G^{\delta}_{3i,j}(\boldsymbol{\xi},t;\mathbf{X},0)\,dV \,. \tag{3}$$

For the analysis here the form of Eq. (2) is more convenient. The surface integral term in Eq. (2) is eliminated by the shallow buried source approximation,[11,24] where the source is considered to act at a small subsurface depth ζ_0, which is set to an infinitesimal value later. For this approximation the stress glut vanishes both on the free surface ($\mathbf{S}_1$ in Fig. 2), and on the portion of the envelope projecting into the material ($\mathbf{S}_2$ in Fig. 2). Therefore, only the volume integral of Eq. (2) need be considered, and,

$$u_3(\mathbf{X},t) = -\int_V \Delta\tau_{ij,j}(\boldsymbol{\xi},t) * G^{\delta}_{3i}(\mathbf{X}-\boldsymbol{\xi},t)\,dV \,, \tag{4}$$

where we have also included explicitly the translation invariance of the Green's functions, $G(\mathbf{X},\boldsymbol{\xi}) = G(\mathbf{X}-\boldsymbol{\xi})$, for the present problem.

The general form of the stress glut is now expressed in terms of the momentary distribution of the temperature rise,

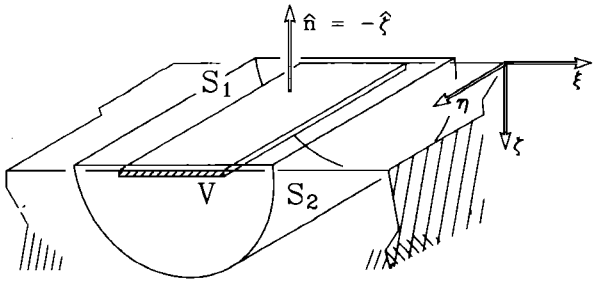

FIG. 2. The thermoelastic surface strip source of volume V. Integration is considered within the half-cylindrical envelope comprising a flat portion S_1 on the material surface boundary, and a cylindrical portion S_2 extending into the material depth.

$\Theta(\xi,t)$, due to the laser heating. Following Scruby *et al.*,[25] Rose[11] and Doyle,[26] the stress-free strain, $\Delta e_{kl}(\xi,t)$, is expressed as

$$\Delta e_{kl}(\xi,t) = \alpha_T \Theta(\xi,t)\delta_{kl} , \tag{5}$$

where α_T is the linear thermal expansion coefficient for the material. Therefore, for an isotropic medium, with Lamé constants, λ and μ, the thermal stress glut is

$$\Delta\tau_{ij}(\xi,t) = \alpha_T(3\lambda + 2\mu)\Theta(\xi,t)\delta_{ij} .$$

Substituting the expression above in Eq. (4), we find

$$u_3(\mathbf{X},t) = -\alpha_T(3\lambda + 2\mu) \times \int_V \frac{\partial}{\partial \xi_i} \Theta(\xi,t) * G^{\delta}_{3i}(\mathbf{X} - \xi,t)dV . \tag{6}$$

Equation (6) is the required integral representation for an extended thermoelastic source at the surface. Nevertheless, for illustrating some of the physical insight discussed in Sec. III, it is more convenient to replace Eq. (6) with its equivalent form, in terms of Green's functions for a point force loading and a Heaviside temporal excitation, G^{H}_{3i}. Denoting differentiation with respect to time with a dot, setting $\mathscr{C} = \alpha_T\ (3\lambda + 2\mu)$, we use the relation $\dot{G}^{H}_{3i} = G^{\delta}_{3i}$, the physical initial conditions $\dot{G}^{H}_{3i} = G^{H}_{3i} = 0$ for $t \leqslant 0$, and the equivalence $f * \dot{g} = \dot{f} * g$, to rewrite Eq. (6) as

$$u_3(\mathbf{X},t) = -\mathscr{C} \int_V \frac{\partial}{\partial \xi_i} \dot{\Theta}(\xi,t) * G^{H}_{3i}(\mathbf{X} - \xi,t)dV . \tag{7}$$

In the following, we will introduce the form of the Green's functions needed to evaluate this function (Sec. I B), and evaluate the momentary temperature profile of the thermoelastic strip source (Sec. I C) to obtain the desired expression for the generated acoustic waveform.

B. Surface displacement Green's functions

Closed-form expressions for G^{H}_{3i} are inferred from solutions for the surface displacement due to a normal[24] and a tangential[27] point load of a semi-infinite, isotropic solid. Inspecting the three functions G^{H}_{3i}, we find that G^{H}_{32} varies as $\sin\theta$, where θ is the angle between the acting force and the line of observation.[27] Consequently, if the observation point is symmetric with respect to the source, the contribution due to G^{H}_{32} are antisymmetric and therefore have no net effect on the vertical displacement. Therefore, in limiting the analysis to sources that are *symmetric* with respect to the line of observation, $x = 0$, all contributions from source loading components acting in the η direction are self canceling.[28] Under this symmetry condition, only two terms in Eq. (4) contribute to the displacement

$$u_3(x, y = z = 0,t) = -\mathscr{C} \int_V \frac{\partial}{\partial \xi} \dot{\Theta}(\xi,t) * G^{H}_{31}(\mathbf{X} - \xi,t)dV - \mathscr{C} \int_V \frac{\partial}{\partial \zeta} \dot{\Theta}(\xi,t) * G^{H}_{33}(\mathbf{X} - \xi,t)dV . \tag{8}$$

Figure 3(a) and (b) plots the vertical displacement of the Green's functions G^{H}_{31}, and G^{H}_{33} as a function of time. The temporal scale is normalized as $\tau = tc_s/r$, where c_s is the shear velocity, and r the distance to the observation point, $\mathbf{X} - \xi$. The normalized arrival times (for a Poisson's Ratio of 0.25) of the longitudinal ($\tau = 1/\sqrt{3}$), shear ($\tau = 1$), and Rayleigh ($\tau = 0.5\sqrt{3 + \sqrt{3}}$) components are indicated on each graph by *P*, *S*, and *R*, respectively.

The Rayleigh components are responsible for the domi-

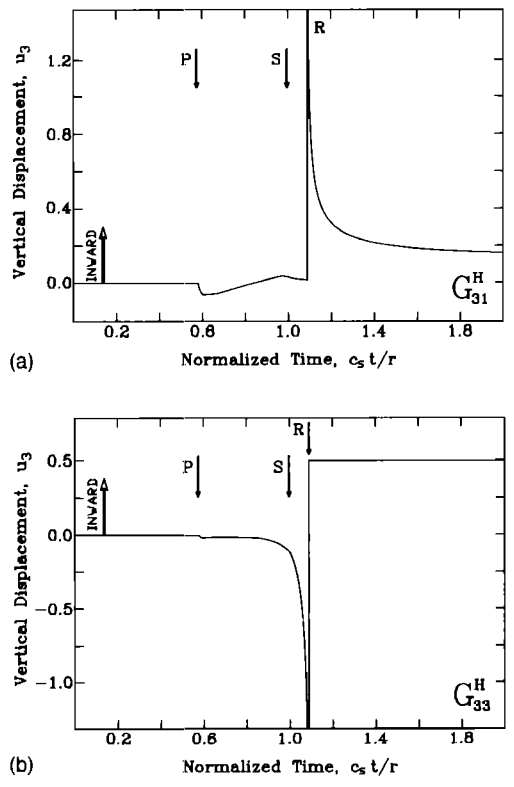

FIG. 3. Vertical displacement due to a unit horizontal (a) or vertical (b) surface point force with a Heaviside function temporal excitation (G^{H}_{31} and G^{H}_{33}, respectively). Ordinate scale is normalized in multiples of $1/\pi\mu r$. The abscissa is plotted in normalized time: $\tau = c_s t/r$. *P*, *S*, and *R* indicate the time of arrival of the longitudinal, shear, and Rayleigh components, respectively.

nant surface perturbation in both cases. As further discussed in Sec. III, the difference in the buildup of the steady-state displacement between G_{31}^{H} and G_{33}^{H} is significant as a verification for the present derivation. For a tangential load an abrupt *sagging* occurs on arrival of the Rayleigh component, followed by a gradual decay to the steady-state value [Fig. 3(a)]. In contrast, a vertical load produces a gradual buildup of an *upward* displacement followed by an abrupt transition to the steady-state value on arrival of the Rayleigh component [Fig. 3(b)]. We emphasize that a *positive* value of u_3 corresponds to material surface *sagging*, so the sign of the steady-state displacements is in agreement with that expected from a static point load on a half-space:[29] the surface sags for both a downward vertical and a horizontal (in the observation direction) point force.

C. Evaluation of the thermal distribution at the source

In order to evaluate Eq. (8) to find the vertical displacement of a symmetric, thermoelastic surface strip source, it remains to derive $(\partial/\partial\xi)\Theta$ and $(\partial/\partial\zeta)\Theta$ for the strip source geometry shown in Fig. 2.

Since the heating light propagates throughout the source dimensions much faster than any time scale of significance here, the temporal heating profile can be considered uniform throughout the source. Therefore, the laser surface heating distribution function can be presented in a normalized, separable form: $Q(\xi,t) = Qh(\xi)q(t)$, where

$$\int_V h(\xi)dV = 1, \quad \int_0^\infty q(t)dt = 1,$$

and Q represents the total *absorbed* heat due to the laser pulse.

The temperature distribution generated by the laser heating is expressed as a superposition of point-source solutions to the heat conduction equation[30] throughout the volume of the extended source, such that

$$\Theta(\xi,t) = \frac{Q}{\rho c_v} q(t) * \int_{V'} h(\xi')\,\Theta^{\delta}(\xi,t;\xi',0)dV', \tag{9}$$

where the point-source solution Θ^{δ} is

$$\Theta^{\delta}(\xi,t;\xi',0) = \frac{1}{(4\pi\kappa t)^{3/2}} \exp\left(-\frac{|\xi-\xi'|^2}{4\kappa t}\right), \tag{10}$$

and where V' and (ξ',η',ζ') are the volume and coordinates of the heat source, and ρ and c_v are the material's density and specific heat, respectively.

In metals the penetration depth of laser radiation is confined to the electromagnetic "skin depth." For example, the penetration is some 5 nm in aluminum and 3 nm in steel[31] for the Nd:YAG laser wavelength, 1.06 μm. Therefore, as long as the thermal diffusion can be neglected, for all practical purposes the thermal source can be considered confined to an infinitesimal depth $\delta(\zeta')$. Nevertheless, for mathematical convenience, we shall assume that the heat penetrates the material to act at a depth of ζ_0, which will later be set infinitesimal. Therefore, the rectangular strip source can be represented in the following form: $h(\xi') = (1/ld) \times \mathrm{rect}(\xi'/d)\mathrm{rect}(\eta'/l)\delta(\zeta'-\zeta_0)$, where $\mathrm{rect}(\xi) \equiv 1$ for $-0.5 \leqslant \xi \leqslant 0.5$ and 0 otherwise. Substituting for $h(\xi')$ in Eqs. (9) and (10), we find

$$\Theta(\xi,t) = \frac{Q}{\rho c_v} q(t) * \frac{1}{ld(4\pi\kappa t)^{3/2}} \int_{-d/2}^{d/2} d\xi' \int_{-l/2}^{l/2} d\eta' \times \exp\left(-\frac{(\xi-\xi')^2 + (\eta-\eta')^2 + (\zeta-\zeta_0)^2}{4\kappa t}\right). \tag{11}$$

The derivatives of Θ, $(\partial/\partial\xi)\Theta$ and $(\partial/\partial\zeta)\Theta$, are found by direct differentiation of Eq. (11):

$$\frac{\partial}{\partial\xi}\Theta(\xi,t) = \frac{-Q}{\rho c_v} q(t) * \frac{1}{ld(4\pi\kappa t)^{3/2}} \times \left[\exp\left(-\frac{(\xi-d/2)^2}{4\kappa t}\right) - \exp\left(-\frac{(\xi+d/2)^2}{4\kappa t}\right)\right] \times \int_{-l/2}^{l/2} d\eta' \exp\left(-\frac{(\eta-\eta')^2}{4\kappa t}\right)\exp\left(-\frac{(\zeta-\zeta_0)^2}{4\kappa t}\right) \tag{12}$$

and

$$\frac{\partial}{\partial\zeta}\Theta(\xi,t) = \frac{Q}{\rho c_v} q(t) * \frac{1}{ld(4\pi\kappa t)^{3/2}} \times \int_{-d/2}^{d/2} d\xi' \exp\left(\frac{(\xi-\xi')^2}{4\kappa t}\right) \times \int_{-l/2}^{l/2} d\eta' \exp\left(-\frac{(\eta-\eta')^2}{4\kappa t}\right) \times \frac{-2(\zeta-\zeta_0)}{4\kappa t}\exp\left(-\frac{(\zeta-\zeta_0)^2}{4\kappa t}\right). \tag{13}$$

These expressions can be simplified by considering the typically minute values of the diffusion length $\sqrt{4\kappa t}$. The thermal conductivity κ varies from $\sim$4 mm^2/s for stainless steel to some 90 mm^2/s for aluminum.[32] Therefore, for a typical Nd:YAG Q-switched laser pulse duration of $t \sim 20$ ns the corresponding diffusion length is in the range of 0.5 to 3 μm, which is some two orders of magnitude below the smallest dimension of interest here. Therefore, the ζ dependence of Eq. (13) is confined to a minute region in the vicinity of ζ_0, and is antisymmetric about this point. Since G_{33}^{H} is virtually independent of ζ for the very small ζ_0/r ratios considered here,[33] the integral over the product $(\partial/\partial\zeta)\Theta G_{33}^{H}$ in the second term of Eq. (8), is null. Consequently, we find that only the tangential load components contribute to the surface displacement for a thermoelastic surface strip generator.

Now setting $\sqrt{4\kappa t} \to 0$, using the Gaussian representation for the Dirac delta function,

$$\delta(x) = \lim_{N\to 0} \frac{1}{\sqrt{\pi}N} \exp\left(-\frac{x^2}{N^2}\right),$$

and letting $\zeta_0 \to 0$, Eq. (12) reduces to

$$\frac{\partial}{\partial\xi}\Theta(\xi,t) \xrightarrow{\zeta_0,\sqrt{4\kappa t}\to 0} \frac{Q}{\rho c_v}\frac{q(t)}{ld}\left[\delta\left(\xi+\frac{d}{2}\right) - \delta\left(\xi-\frac{d}{2}\right)\right] \times \mathrm{rect}(\eta/l)\delta(\zeta). \tag{14}$$

Substituting for $(\partial/\partial\xi)\Theta$ from Eq. (14) into Eq. (8), we find

$$u_3(x,y=z=0,t) = \frac{-\alpha_T(3\lambda+2\mu)Q}{\rho c_v l d}\dot{q}(t) * \int_{-l/2}^{l/2} d\eta \times\left[G_{31}^{H}\left(x+\frac{d}{2},\eta,\zeta=0,t\right) - G_{31}^{H}\left(x-\frac{d}{2},\eta,\zeta=0,t\right)\right]. \quad (15)$$

This result shows that the thermoelastic strip source is effectively equivalent to two line sources of horizontal forces acting outwards along its edges ($\xi = \pm d/2$). The magnitude of each force per unit length is $\alpha_T(3\lambda+2\mu)Q/(\rho c_v l d)$, indicating that the amplitude of the ultrasound depends only on the heat flux Q/ld into the source and not on the source dimension d or l.

D. The short thermoelastic surface strip source

The surface displacement waveform can be evaluated directly from Eq. (15). However, for several applications it is sufficient to consider only the leading-edge portion of each pulse.[4] In this case, the effects of the far–off-axis contributions of the source may be neglected, significantly reducing the computation load. This short (in the lateral, η dimension) strip approximation is considered below; long strips are considered in the proceeding section.

The leading rise times of the laser-generated signals are typically shorter[4] than the other components of the acoustic waveform. Therefore, contributions from the lateral edges of the source, which are delayed by longer trajectories, cannot be expected to affect the signal's *leading* edge. For example, in the experimental geometry used here, the far–off-axis contributions arrive after $[\sqrt{(l/2)^2+r^2}-r]/c_R \sim 300$ ns; too late to affect typical experimental leading-edge rise times (50 ns). Therefore, only the portion of the source close to the line of observation significantly affects the leading-edge rise time. This phenomenon is verified numerically in Sec. I E, and experimentally in Sec. II below.

For the short-strip approximation, that is $l \ll r$, Eq. (15) reduces to

$$u_3^{(s)}(x,t) = \frac{\alpha_T(3\lambda+2\mu)Q}{\rho c_v d}\dot{q}(t) * \left[G_{31}^{H}\left(x-\frac{d}{2},t\right) - G_{31}^{H}\left(x+\frac{d}{2},t\right)\right], \quad (16)$$

where the integration of the lateral extent is eliminated. This result, plotted for $q(t)=\delta(t)$ in Fig. 4, shows that the polarity in the leading and trailing edges of the acoustic displacement are reversed in sign, and separated by the transit time across the source's width d.

For the purpose of comparing the results with experimental waveforms, Eq. (16) is evaluated for the temporal profile $q(t)$ that matches the empiric trace of the Nd:YAG Q-switched laser pulse used in the experimental work[4] [Fig. 5(a)], and for the source proportions used in the experimental work: $d = 0.15r$. Numerical integration of Eq. (16), with

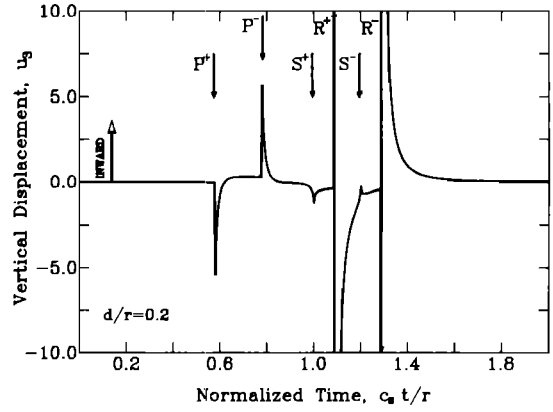

FIG. 4. Vertical surface displacement due to a short thermoelastic surface strip of width $d = 0.2r$ and δ function time dependence. Abscissa: normalized time $\tau = c_s t/r$. Ordinate: vertical surface displacement, normalized in multiples of $\alpha_T(3\lambda+2\mu)Q/(\pi\mu\rho c_v dr)$. P^+, S^+, and R^+ denote the arrival times of the longitudinal, shear, and Rayleigh component peaks of the leading wave front, respectively. The same components for the trailing edge are marked as P^-, S^-, and R^-.

suitable treatment of the discontinuities in G_{31}^{H},[28] yields the waveform shown in Fig. 6. This signal, which is dominated by the Rayleigh components, is consistent with the point-source solution[11] in two respects. For $d \to 0$ the source is reduced to a tangential surface dipole, as expected.[8,11] In addition, numerical convolution of the theoretical point-source solution with the width of the generating strip yields an identical waveform to that presented in Fig. 6. Further experimental confirmation is described in the following.

The irregular form of the negative portion of each of the pulses is due to the nonmonotonic decay of the empiric pulse profile [Fig. 5(a)]. This is demonstrated by comparing in Fig. 7 numerical waveforms for the two temporal profiles $q(t)$ shown in Fig. 5: the empiric pulse and a Gaussian pulse of similar half-peak-intensity width. In both cases, the signal comprises two antisymmetric pulses that originate from the opposite edges of the source, and on the assumption that d is large enough to ensure their separation, only the leading

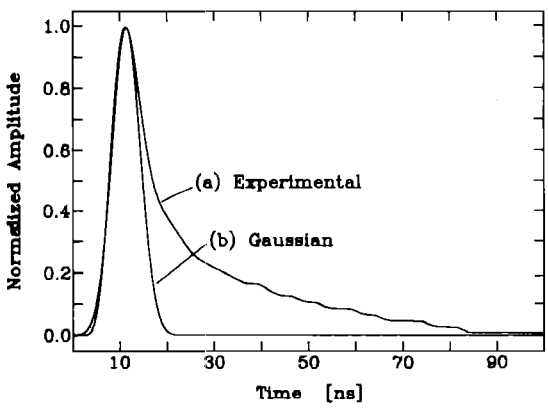

FIG. 5. Experimental temporal profile for the Q-switch Nd:YAG laser used (a) compared to a Gaussian temporal profile with $\sigma_t = 6$ ns, (b). Both signals are normalized to a unit amplitude.

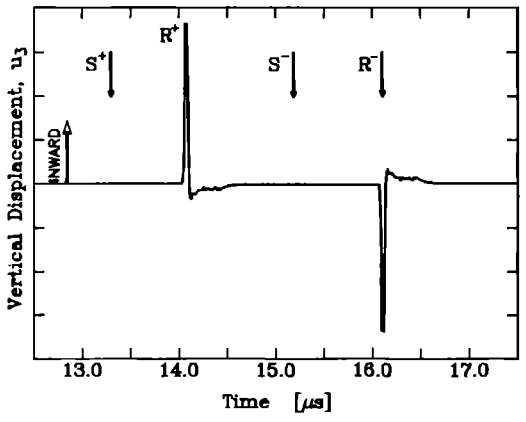

FIG. 6. Vertical surface displacement due to a thermoelastic strip source with $d = 0.15r$ ($r = 41$ mm) for the experimental laser temporal profile. S^+, R^+, S^-, and R^- denote the arrival times of the shear and Rayleigh components, for the leading and trailing edges of the strip respectively. The ordinate is in arbitrary units.

pulse of each is shown. In both cases, the Rayleigh component dominates, and the leading portion of the signals assume the form of the derivative of the temporal excitation $\dot{q}(t)$, then gradually decay to the zero-displacement steady state. As discussed further in Sec. III, these characteristics are related to the abrupt nature of the leading edge of G_{31}^{H} as compared to the gradual decay of this function's trailing edge [Fig. 3(a)].

E. Long thermoelastic strips

The derivation leading to Eq. (15) established that only the edges of the thermoelastic strip source contribute to the acoustic displacements. A particularly simple mathematical form for the resulting waveforms is obtained if the lateral extent of the source is sufficiently short. The present section considers long strip sources, showing that the extended length mainly affects the *trailing* signal portions.

In order to incorporate the effect of the lateral extent of the source it is necessary to perform the integration over η in Eq. (15). Nevertheless, since a solution for a short strip is already available, we choose to regard the long strip as a superposition of a series of contiguous, short strips distributed along the strip's length l. This is equivalent to a series of outward acting point sources, distributed along the two edges of the strip, $\xi = \pm d/2$, as shown schematically in Fig. 8(a). To evaluate the long strip displacement, $u_3^{(l)}$, each short strip contribution at the observation point must be weighted by $\cos\theta$, the angular dependence of G_{31}^{H};[27] attenuated by α; and phase shifted by ϕ, to account for the additional trajectory, Δr (cf. Fig. 8):

$$u_3^{(l)}(x,t) = \int_{-l/2}^{+l/2} u_3^{(s)}(x, t-\phi)\alpha \cos\theta \, d\eta , \qquad (17)$$

where

$$\theta = \tan^{-1}(\eta/r) ,$$

$$\phi = \frac{\Delta r}{c_R} = \frac{\eta}{c_R} \tan\left(\frac{\theta}{2}\right) ,$$

and

$$\alpha \sim \sqrt{r/(r+\Delta r)} .$$

Only the $r^{-1/2}$ attenuation rate of a Rayleigh wave is used here, since the other components, which are attenuated faster,[33] have virtually no effect on the resulting waveform.

Figure 9(a) and (b) present results of numerical integration of Eq. (17) for a number of source lengths and for the empirical Nd:YAG temporal profile and a Gaussian temporal excitation, respectively. Only the leading acoustic pulse is shown, representing the full waveform with its two antisymmetric pulses (which are essentially independent for sufficiently large d). The amplitudes of the signals are normalized to the same peak-to-peak value to facilitate comparison between the rise times of the pulses. Virtually no pulse-width broadening occurs for source lengths of $l \leqslant 0.1r$. For longer strips, only the *trailing* portion of the pulses change appreciably. It is very striking that the leading-pulse rise times are essentially unaffected by the lateral extent of

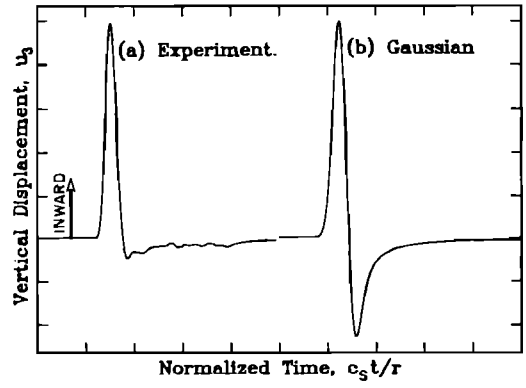

FIG. 7. Rayleigh component of vertical surface displacement due to the leading edge of the thermoelastic strip source. (a) Experimental laser temporal profile, (b) Gaussian temporal profile. Abscissa: normalized time $\tau = c_s t/r$, at 0.01 per division. Ordinate: vertical displacement, in arbitrary units.

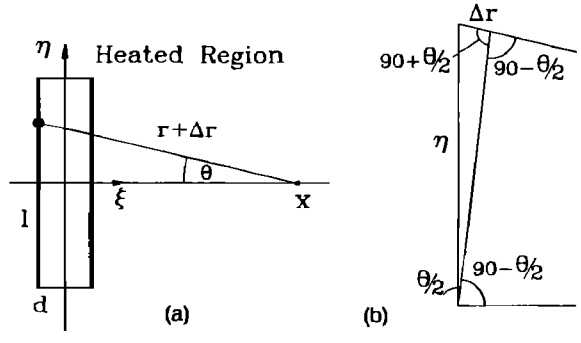

FIG. 8. Long thermoelastic strip source geometry: (a) top view showing the contributing line sources as bold lines; (b) magnified view showing the geometrical construction to evaluate Δr.

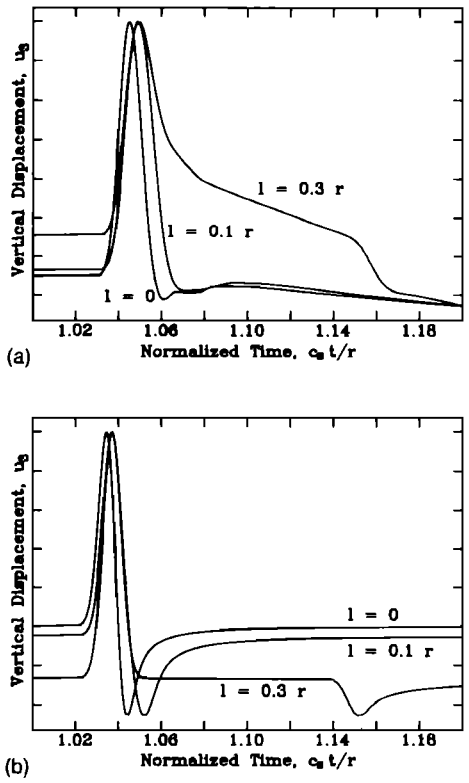

FIG. 9. Numerical estimation of the effect of the lateral extent of the illumination strip for: (a) Experimental temporal profile, (b) Gaussian temporal profile. The waveforms are normalized to equal peak-to-peak values for comparison of the temporal characteristics.

the source. Interestingly, for the Gaussian temporal excitation the negative portion of the pulse is separated from the leading positive portion for large l values [Fig. 9(a)]. A significantly different trailing edge form is found for the empirical temporal profile [Fig. 9(b)].

II. EXPERIMENTAL

In this section, we present experimental waveforms generated by a thermoelastic strip source, and compare them to those predicted by the theoretical model. The experimental arrangement, in which the ultrasound is generated and detected on a polished aluminum slab, is shown in Fig. 10. An expanded Q-switched Nd:YAG laser beam, with 6-ns pulse rise time [cf. Fig. 5(a)], and 480-mJ pulse energy is the thermal source. A rectangular aperture confines the surface illumination to a strip of $d = 6$-mm width and $l = 16.5$-mm lateral extent. The illumination across the strip is nearly uniform with a peak incident flux on the order of 1 MW/cm^2. The ultrasound generated by the Nd:YAG pulse is detected $r = 41$ mm away from the source with a focused, 7-mW HeNe laser beam. Using the knife-edge (KE) technique[34] the surface *slope* due to the ultrasound traversing the detection point, is recorded with a high-speed digital transient recorder.

A typical KE detected experimental signal is compared in Fig. 11 to the theoretical *slope* predicted by the derivative of the vertical surface displacement for a *short strip*:

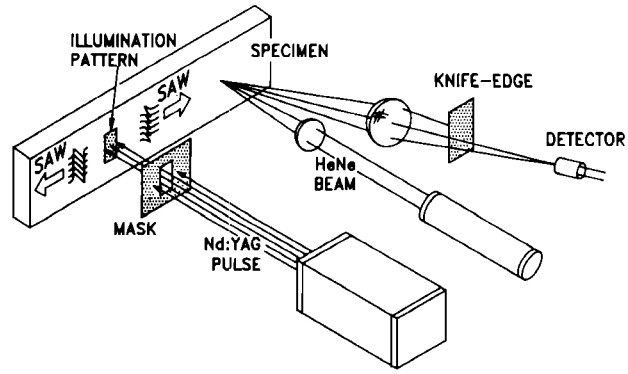

FIG. 10. Perspective illustration of the experimental arrangement.

$(\partial/\partial t)u_3^{(s)}$ of Eq. (16). To remove the error due to uncertainty in the system's detection gain, the amplitude of the theoretical waveform is rescaled to fit the peak of the first positive pulse in the experimental signal. The similarity between these waveforms is notable. The model predicts correctly the salient features of the experimental waveform, including its polarity, and the antisymmetry of the two separate bipolar pulses. The longitudinal (not shown in Fig. 11) and the shear displacement components (marked $S^{\pm}$ in Fig. 11) are too weak to be discerned in both the experimental as well as the theoretical waveforms. The experimental signal in Fig. 11 is generated by a strip with $l = 0.4r$, and therefore shows some deviation from the short strip approximation in the trailing portions of the pulses, most notably in the second pulse. As for the leading-edge rise time, its theoretical invariance with the source's lateral extent was verified empirically: No change in the pulse's rise time is observed when the lateral extent of the illumination strip, l is varied. Furthermore, no change in the pulse's width is notable for $l \leqslant 0.2r$.

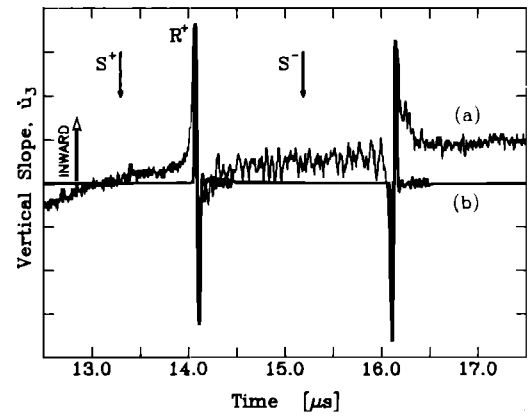

FIG. 11. A comparison of (a) experimental and (b) theoretical waveforms for the surface *slope* due to a short thermoelastic surface source ($d = 6$ mm, $r = 41$ mm) and the empirical laser temporal profile. S^+, R^+, S^-, and R^- denote the arrival times of the shear and Rayleigh components, for the leading and trailing edges of the strip, respectively. The experimental waveform is the average of signals from four consecutive laser pulses. The ordinate is in arbitrary units.

III. DISCUSSION

The main contribution of this work is a formulation of a model for the ultrasonic surface waveforms generated by a thermoelastic strip source. If the thermoelastic strip is short, that is $l \leqslant 0.1r$, a particularly simple form is predicted for the acoustic signals [Eq. (16)]. This form is also a good approximation for the leading portions of longer strips, and only if a more accurate evaluation of the trailing portions of each acoustic pulse is required, an additional integration, such as described by Eq. (17), is necessary. These models further emphasize the substantial practical advantages of the strip source,[3,4] as discussed later on in this section.

The theoretical model provides a means of predicting the true waveform of the thermoelastic strip source prior to any material degrading effects it may experience in propagating to the detection point. For example, for dispersive material, the detected waveform is spectrally distorted; using the theoretical model as a reference, the frequency-dependent attenuation can be measured, from which important material parameters, such as grain size can be extracted.[4] The simplicity of the numerical form is an advantage for parameter estimation procedures requiring iterative fitting of theoretical waveforms to experimental data.[4] This ability to relate the experimental waveform parameters to *quantitative* material properties has been successfully employed both for *absolute* measurements of material grain size[4] and monitoring the combined effects of material texture and residual stress.[28]

The analysis here predicts that the waveform generated by the thermoelastic strip source is independent of the material's *thermal* properties. This is borne by the form of Eq. (15), in which all the thermal parameters occur only in the scaling coefficient. A related property was observed by Rose,[11] who proved that, for a point, adiabatic source, the acoustic disturbance form depends soley on the spatial and temporal profiles of the thermal *source*, and not on the momentary thermal distribution. This result can be extended to apply to the thermoelastic strip source.[28] In practice, this independence of thermal properties, alleviates the need to calibrate for them while monitoring mechanical or metallurgical material properties. We note that this would not apply to any signal contributions due the thermal diffusion,[21] which is neglected in our analysis.

The salient feature of the theoretical and the experimental waveforms, agree well as shown in Fig. 11. In both the Rayleigh component dominates;[8,11,35] two, antisymmetric bipolar pulses occur, separated by the acoustic propagation delay across the thermoelastic strip width; and the material initially *sags*. For the aluminum sample, which has negligible dispersion in the frequency range used here, the theoretical and experimental leading-edge signal rise times are also well correlated. In general,[3,4,28] lesser correlation is observed for the trailing edges of each acoustic pulse, as can be expected from the relatively long strip sources used.

The elimination of the vertical components in the thermal source warrants a closer examination. One can expect no vertical forces on the free boundary, so for the small laser penetration depth, this result is intuitively acceptable. Analytically, the equivalence of a thermoelastic surface point source and a tangential force dipole[11] confirms this result. The experimental evidence[8] also supports the same effect. The different characteristics of the vertical and tangential Green's functions make the experimental observations significant; the Rayleigh components of G_{31}^{H} and G_{33}^{H} are similar but inverted in polarity with respect to each other (Fig. 3). Therefore, the agreement between the theoretical and experimental waveforms indicate that the source is dominated by tangential forces, if not verifying the complete negation of the vertical contribution.

The analysis confirms two of the unique practical advantages of the thermoelastic strip source: the high amplitudes and the very high-frequency content of the resulting waveforms. As described below, both are independent of the source's width, and are not affected by small nonuniformities in the source's cross section.

Considering the amplitude, the theoretical model predicts that it is determined by the *time derivative* of the incident laser pulse profile $\dot{q}(t)$ in agreement with a different acoustothermal model due to Budenkov.[36] Mathematically this can be inferred from Eq. (16), where the dominant effect of G_{31}^{H} can be, somewhat coarsely, represented by a delta function [cf. Fig. 3(a)]. Consequently, the convolution integral $\dot{q}*G_{31}^{H}$ essentially reduces to $\dot{q}(t)$. Intuitively, it is reasonable that a higher heating rate would induce a greater thermal strain, and therefore a larger ultrasonic amplitude. This property of the strip source explains the difference between the negative signal potions for the empirical and Gaussian temporal excitations in Fig. 7. The slower decay rate of the empirical excitation [Fig. 5(a)] results in its weaker negative component.

Therefore, in practice, the optical heat deposition rate, rather than the optical flux, governs the resulting ultrasonic amplitudes. Substantial amplitude increases are possible just by shortening the optical pulse rise time. Such large amplitudes are important for improved detection accuracies, which are typically related to the signal-to-noise ratio, and scale with the available peak amplitudes. Another practical advantage is the independence of the acoustic amplitudes on the dimensions of the generating thermal strip. As noted in Sec. I C only the heating flux, Q/ld, affects the generated amplitude. Again, this result relates to the dependence of the acoustic amplitudes, on the thermal strain rate, which is maximized at the thermoelastic strip's edges. Therefore, the thermoelastic strip edges generate the maximal possible acoustic disturbance which would not typically be affected by small variations in the uniformity of the illumination within the strip, nor its width.

The high-frequency content also results from the singularity in the Green's function in Eq. (16). Since G_{31}^{H} features an abrupt step on arrival of the Rayleigh component [Fig. 3(a)], its convolution with $\dot{q}(t)$ replicates the rise time of $\dot{q}(t)$. In other words, irrespective of the material parameters, the leading-edge rise time of the strip-generated ultrasound is identical to that of the leading edge of the optical pulse derivative; laser pulse derivatives can readily be obtained on a nanosecond scale, or even substantially faster.

Due to the relatively fast rise times possible with the

thermoelastic strip source, the resulting ultrasonic frequency content is substantially higher than that possible with a gradual surface illumination intensity distribution (Gaussian for instance) or a convex front-end geometry (disk for example). Furthermore, the frequency content, or leading rise time are virtually independent of both the widths as well as the lateral extent of the strip (Sec. I E). They are also insensitive to small inhomogeneities in the illumination profile, as long as a well-defined illumination boundary occurs. In as much as the incident laser pulse profile is known, this property ensures a *calibrated* ultrasonic rise-time signature, which is invaluable for many high-frequency applications.

IV. CONCLUSIONS

A practical theoretical model for the ultrasonic waveforms generated by the thermoelastic surface strip source is derived. The model correctly describes the main experimental features: the dominance of the Rayleigh component, the two, antisymmetric pulses, the pulse separation, d/c_R and their polarity. The model also demonstrates the practical advantages of the thermoelastic strip source, including large amplitudes, and a high-frequency content. Both of these parameters are essentially independent of the strip's dimensions (provided a minimal width is exceeded) and insensitive to inhomogeneities in its illumination profile. Furthermore, both the amplitude and the leading-edge rise times are proportional to the heat deposition rate, so that faster optical excitation pulses can improve the performance of time- or frequency-domain measurements. In significantly reducing the computational load, the model can readily be applied to iterative parameter estimation procedures that optimize the accuracy of ultrasonic nondestructive evaluation and testing methods.

The thermoelastic strip source, complemented by the model presented above, is an important tool for qualitative and quantitative nondestructive material evaluation. So far we have applied it to accurate ultrasonic time-of-flight measurements for monitoring the combined effects of residual stress and material texture;[28] to the *absolute* measurement of frequency-dependent attenuation from which accurate material grain size and absorption coefficients were obtained;[4] and to the detection of fatigue microcracks which invert the polarity of high-frequency ultrasound.[28]

ACKNOWLEDGMENTS

This work was supported by the National Council for Research and Development, Israel, by The Directorate General for Science Research and Development of the Commission of the European Communities (Contract No. 2507), and by industrial sources associated with Tel Aviv University.

[1]C. B. Scruby, F. K. Brocklehurst, B. C. Moss, and D. J. Buttle, "Some recent applications of laser ultrasound to the characterization of materials," Nondestruct. Eval. **5**, 97–119 (1990).

[2]J. -D. Aussel and J.-P. Monchalin, "Study of surface acoustic wave dispersion using laser-ultrasonics and applications to thickness measurement," *Review of Progress in Quantitative Nondestructive Evaluation*, edited by D. O. Thompson and D. E. Chimenti (Plenum, New York, 1989), Vol. 8, pp. 535–542.

[3]A. Aharoni, M. Tur, and K. M. Jassby, "Laser based transduction of ultrasound for practical NDT applications," SPIE **1038**, 265–272 (1988).

[4]A. Aharoni, M. Tur, and K. M. Jassby, "Monitoring material grain size by laser generated ultrasound," Appl. Phys. Lett. **59**, 3530–3532 (1991).

[5]R. M. White, "Generation of elastic waves by transient surface heating," J. Appl. Phys. **34**, 3559–3567 (1963).

[6]H. M. Ledbetter and J. C. Moulder, "Laser-induced Rayleigh waves in aluminum," J. Acoust. Soc. Am. **65**, 840–842 (1979).

[7]C. B. Scruby, R. J. Dewhurst, D. A. Hutchins, and S. B. Palmer, "Quantitative studies of thermally generated elastic waves in laser-irradiated metals," J. Appl. Phys. **51**, 6210–6216 (1980).

[8]C. B. Scruby, R. J. Dewhurst, D. A. Hutchins, and S. B. Palmer, "Laser generation of ultrasound in metals," in *Research Techniques in Nondestructive Testing* (Academic, New York, 1982), Vol. 5, p. 281.

[9]R. J. Dewhurst, D. A. Hutchins, S. B. Palmer, and C. B. Scruby, "Quantitative measurements of laser-generated acoustic waveforms," J. Appl. Phys. **53**, 4064–4071 (1982).

[10]D. A. Hutchins, R. J. Dewhurst, and S. B. Palmer, "Directivity patterns of laser-generated ultrasound in aluminum," J. Acoust. Soc. Am. **70**, 1362–1369 (1981).

[11]L. R. F. Rose, "Point-source representation for laser-generated ultrasound," J. Acoust. Soc. Am. **75**, 723–732 (1984).

[12]C. Chang and W. Sachse, "Analysis of elastic wave signals from an extended source in a plate," J. Acoust. Soc. Am. 77, 1335–1341 (1985).

[13]C. M. Scala and P. A. Doyle, "Time- and frequency-domain characteristics of laser-generated ultrasonic surface waves," J. Acoust. Soc. Am. **85**, 1569–1576 (1989).

[14]P. A. Doyle, "Calculation of ultrasonic surface waves from an extended thermoelastic laser source," J. Nondestr. Eval. **8**, 147–164 (1989).

[15]L. F. Bresse and D. A. Hutchins, "Transient generation by wide thermoelastic source at a solid surface," J. Appl. Phys. **65**, 1441–1446 (1985).

[16]J. -D. Aussel, A. Le Brun, and J. C. Baboux, "Generating acoustic waves by laser: theoretical and experimental study of the emission source," Ultrasonics **26**, 245–255 (1988).

[17]U. Schleichert, M. Paul, B. Hoffmann, K. J. Langenberg, and W. Arnold, "Theoretical and experimental investigations of broadband thermoelastically generated ultrasonic pulses," in *Photoacoustic and Photothermal Phenomena, Springer Series in Optical Sciences* (Springer-Verlag, Berlin, 1988), Vol. 58, pp. 284–287.

[18]U. Schleichert, M. Paul, B. Hoffmann, K. J. Langenberg, and W. Arnold, "A quantitative theory of laser-generated ultrasound," Proc. Conf. Review of Progress in NDE, La Jolla, July 31–Aug. 3 (1988).

[19]S. Fassbender, M. Kulkov, B. Hoffmann, M. Paul, H. Peukert, and W. Arnold, "Efficient generation of acoustic pressure waves by short laser pulses," Proc. Conf. European Materials Research Soc., Strassbourg, Paper No. C-III.4 (1989).

[20]B. A. Boley and J. H. Weiner, *Theory of Thermal Stresses* (Wiley, New York, 1960).

[21]F. A. McDonald, "On the precursor in laser-generated ultrasound waveforms in metals," Appl. Phys. Lett. **56**, 230–232 (1990).

[22]G. Bachus and M. Mulcahy, "Moment tensors and other phenomenological descriptions of seismic sources—I: Continuous displacements," Geophys. J. R. Astron. Soc. **46**, 341–361 (1976).

[23]K. Aki and G. Richards, *Quantitative Seismology* (Freeman, San Francisco, 1980), Vol. 1.

[24]C. L. Pekeris, "The seismic surface pulse," Proc. Natl. Acad. Sci. (USA) **41**, 469–480 (1955).

[25]C. B. Scruby, H. N. G. Wadley, and J. J. Hill, "Dynamic elastic displacements at the surface of an elastic half-space due to defect sources," J. Phys. D: Appl. Phys. **16**, 1069–1083 (1983).

[26]P. A. Doyle, "On epicentral waveforms for laser-generated ultrasound," J. Phys. D: Appl. Phys. **19**, 1613–1623 (1986).

[27]C. -C. Chao, "Dynamical response of an elastic half-space to tangential surface loadings," J. Appl. Mech. **27**, 559–567 (1960).

[28]A. Aharoni, "Laser-based methods for generation and detection of ultrasound with practical nondestructive testing applications," Ph. D. thesis, Tel Aviv University, Tel Aviv 69978, Israel (1990).

[29]S. P. Timoshenko and J. N. Goodier, *Theory of Elasticity* (McGraw-Hill, New York, 1970).

[30]H. S. Carslaw and J. C. Jaeger, *Conduction of Heat in Solids* (Oxford U. P., Oxford, 1959).

[31]B. I. Bleaney and B. Bleaney, *Electricity and Magnetism* (Oxford U. P., Oxford, 1965).
[32]F. Kreith, *Principles of Heat Transfer* (International Textbook Co., Scranton, PA, 1958).
[33]C. L. Pekeris and H. Lifson, "Motion of the surface of a uniform elastic half-space produced by a buried pulse," J. Acoust. Soc. Am. **29**, 1233–1238 (1957).
[34]A. Aharoni, A. Gover, and K. M. Jassby, "Near-field analysis of the knife-edge technique," Appl. Opt. **18**, 3018–3027 (1985).
[35]C. Edwards and S. B. Palmer, "Mathematical modelling of laser generated surface waves," Nondestr. Test. Eval. **5**, 203–22 (1990).
[36]G. A. Budenkov, "Generation of elastic waves in an elastic half space by thermal excitation," Defectoskopiya **3**, 75–81 (1979).